文章编号：0253-374X(2019)S1-0026-06
DOI：10. 11908/j. issn. 0253-374x. 19733

二维类车体尾迹中的低频震荡

黄光远[1,2]，LEUNG Chi Kin Randolph[2]，杨志刚[1,3]，SEID Ka Him[2]
(1. 同济大学 上海市地面交通风洞中心，上海 201804；2. 香港理工大学 机械学院，香港特别行政区 999077；
3. 北京民用飞机技术研究中心，北京 102401)

摘要：汽车尾部的大尺度流动分离是汽车外流场的显著特征之一，其与气动阻力、结构振动和震荡密切相关。应用直接数值模拟(DNS)方法研究在雷诺数$Re=2.3\times10^4$下某二维类车体尾迹中的低频震荡。该类车体常被用于汽车空气动力学学术研究，因为其轮廓可涵盖到货车主要几何特征，且其尾迹与货车的准二维尾迹具有共性。计算结果对照现有的实验结果进行验证，二者之间的差异经过评估确认了该计算的正确性。流场结果显示低频震荡与尾迹中两种模态之间的相互转换有关。这两种模态分别由Kelvin—Helmholtz不稳定性及尾迹的不稳定性主导。前种模态下，尾部分离的上、下剪切层在几乎相同的时刻产生涡脱落；而在后种模态下，上、下剪切层交替地产生涡脱落形成卡门涡。根据不稳定性理论讨论了模态转换的机理，并阐述了因低频震荡而产生的气动力变化。

关键词：钝体空气动力学； 直接数值模拟； D形体
中图分类号：O351 **文献标志码**：A

Study of Low-frequency Oscillation in the Wake of a Two-dimensional Generic Vehicle Profile

HUANG Guangyuan[1,2], *LEUNG Chi Kin Randolph*[2], *YANG Zhigang*[1,3], *SEID Ka Him*[2]
(1. Shanghai Automotive Wind Tunnel Center, Tongji University, Shanghai 201804, China; 2. Department of Mechanical Engineering, The Hong Kong Polytechnic University, Hong Kong 999077, China; 3. Beijing Aeronautical Science and Technology Research Institute, Beijing 102211, China)

Abstract: Flow around road vehicles is characterized by a massive wake, which is related to aerodynamic drag, unsteady loading, wind noise et al. Therefore, good understanding of the wake dynamics is important. In the present work, a low-frequency oscillation in the wake of a two-dimensional generic vehicle profile is investigated at a reasonably high Reynolds number $Re=2.3\times10^4$ by direct numerical simulation (DNS). Although flow around vehicles is three-dimensional, some flow features are quasi-two-dimensional, such as separations over the head and over a straight back, for which a two-dimensional profile can be used. The flow solution is validated against the existing experimental data, and the calculation presents capacity for capturing dominant flow structures. Results show that a low-frequency oscillation is observed in the amplitude of the lift fluctuation. Other governing properties are also found varying, corresponding to the lift signal at the low frequency. The evolution of the wake during the high- and low-amplitude periods is examined, illustrating the greater lift fluctuation corresponds to the alternative vortex shedding, while the weaker fluctuation corresponds to the simultaneous vortex shedding. The velocity at the upper and the lower shear layers and the surface pressure acting on the trailing edges are comprehensively investigated, indicating the attenuated lift fluctuation is because the surface pressure acting on the upper and the lower sides cancel out, as vortices are shed simultaneously. The mechanism of the exitance of two shedding modes is discussed based on the instabilities of the shear layer and the wake, respectively.

Key words: bluff-body aerodynamics; direct numerical simulation; D-shaped body

Flow around road vehicles separates at the blunt back, leading to a massive wake. The wake dynamics is related to the aerodynamic drag, unsteady loading, wind noise, et al., which are mostly undesired for producers and passengers [1]. Therefore, good understanding of the wake dynamics is essential for the vehicle aerodynamic design. In

收稿日期：2019-06-21
第一作者：黄光远(1992—)，男，博士生，主要研究方向为流体力学。E-mail：97huang@tongji. edu. cn
通信作者：杨志刚(1961—)，男，教授，博士生导师，工学博士，研究方向为流体力学。E-mail：zhigangyang@tongji. edu. cn

previous research, a two-dimensional generic vehicle profile has been popularly used to study the wake dynamics and develop flow control techniques. The profile effectively presents some broad features of the cross-section profile of trucks. Even though flow around road vehicles is three-dimensional, it is capable to employ the profile to study some quasi-two-dimensional flow structures appearing in the vehicle wake, such as rolling-up of the shear layer and von Karman-like vortex street. In the numerical work of Parkin et al., a low-frequency oscillation was observed in the amplitude of the lift fluctuation [2]. They attribute the oscillation to two wake modes: a high-energy mode with larger shear-layer fluctuation, and a low-energy mode with smaller shear-layer fluctuation.

The present work provides an extended study of the wake dynamics of the two-dimensional generic vehicle profile, aiming to understand how the wake modes creates the low-frequency oscillation, and why two modes exist in the wake.

1 Methodology

1.1 Governing equation

Three-dimensional structures are observed in the flow around the generic vehicle profile [3]. Therefore, the flow field is governed by three-dimensional compressible Navier-Stokes equations. However, it is highly expansive to directly solve the equations with accessible computational resources. Given the flow features that we focus, i. e. separations, rolling-up shear layers, and vortex shedding, are found predominated two-dimensional, it allows two-dimensional models to approximate the flow field in order to compromise the computational resources [3]. Based on this line, two-dimensional compressible Navier-Stokes equations are employed to model the flow field. The equations, together with the state equation of ideal gas, can be expressed in a strong conservation form as

$$\frac{\partial \boldsymbol{U}}{\partial t}+\frac{\partial(\boldsymbol{F}-\boldsymbol{F}_v)}{\partial x}+\frac{\partial(\boldsymbol{G}-\boldsymbol{G}_v)}{\partial y}=0 \qquad (1)$$

where $\boldsymbol{U}=\left[\rho\ \rho u\ \rho v\ \rho E\right]^{\mathrm{T}}$, $\boldsymbol{F}=\left[\rho\ \rho u^2+p\ \rho uv\ (\rho E+p)u\right]^{\mathrm{T}}$, $\boldsymbol{G}=\left[\rho v\ \rho uv\ \rho v^2+p\ (\rho E+p)v\right]^{\mathrm{T}}$, $\boldsymbol{F}_v=(1/Re)\left[0\ \tau_{xx}\ \tau_{xy}\ \tau_{xx}u+\tau_{xy}v-q_x\right]^{\mathrm{T}}$, $\boldsymbol{G}_v=(1/Re)\left[0\ \tau_{yx}\ \tau_{yy}\ \tau_{yx}u+\tau_{yy}v-q_y\right]^{\mathrm{T}}$, $\tau_{xx}=(2/3)\mu(2\partial u/\partial x-\partial v/\partial y)$, $\tau_{yy}=(2/3)\mu(2\partial v/\partial y-\partial u/\partial x)$, $\tau_{xy}=\tau_{yx}=\mu(\partial u/\partial y-\partial v/\partial x)$, $E=p/[\rho(\gamma-1)]+(u^2+v^2)/2$, $q_x=-(\mu\partial T)/[(\gamma-1)P_rM^2\partial x]$, $q_y=-(\mu\partial T)/[(\gamma-1)P_rM^2\partial y]$, $P_r=0.7$, and $\gamma=1.4$. The dimensionless equations, with length normalized by the reference height $\hat{H}$ (the hat referring to dimensional variable), velocity by the free stream velocity $\hat{U}_\infty$, density by the free stream density $\hat{\rho}_\infty$, time by $\hat{H}/\hat{U}_\infty$, and pressure by $\hat{\rho}_\infty\hat{U}_\infty^{\ 2}$, are solved using Conservation Element and Solution Element (CE/SE) method [4]. The method has shown high accuracy in calculating separation flows of T-junction merging flow, cavity flow, and flow around a square cylinder flow [5-6].

1.2 Problems setup and computational setup

The problem setup is shown in Fig. 1: a generic vehicle profile, presenting a rectangular cylinder with rounded head, is placed in a uniform flow. The same geometry and dimensions have been used in experiment study by Pastoor [3], and numerical studies by Krajnovic & Fernandes [7], Parkin [2], et al. The Reynolds number, based on the body height H and free-stream velocity U_∞, is chosen to be $Re=23\,000$ in order to compare with the previous research. And a low Mach number $M=0.2$ is prescribed.

Fig. 1 also demonstrates the computational domain. The origin o of a Cartesian coordinate is placed at the center of the back with x- and the y-axials parallel to the streamwise and the transvers directions, respectively. The computational domain is divided into two parts: an inner physical domain and an outer buffer zone. The buffer zone is applied to removing erroneous numerical reflection. The space of the computational domain is discretized by non-uniform meshes. In vicinity of the surface, the

spacing is refined to solve boundary layers on the body surface. The mesh size in the boundary layer is $\Delta x = 0.011$, which corresponds to a dimensionless wall value $y^+ = 13$. In the wake region, the spacing is refined to ensure that a vortex structure is solved by at least 40×40 meshes. No-slip solid wall boundary condition is imposed at body surfaces and non-reflection boundary condition is imposed at outer boundaries.

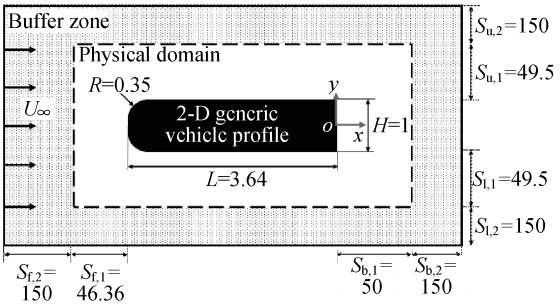

Fig 1 Schematic of the problem setup and the computational domain (dimensions not to scale).

1.3 Validation

Tab. 1 shows results obtained from the present calculation (P), together with results of previous experimental and numerical studies of Pastoor [3] (A), Krajnovic & Fernandes [7] (B), and Parkin [2] (C). The 99% boundary layer thickness δ fits well with the experimental result by a difference of 8.70%. The shape factor is $H_{12} = 1.46$, indicating the turbulent feature of the boundary layer. The difference between the experimental and the numerical results is probably due to the subscale turbulence in the boundary layer. The time-averaged drag coefficient $\overline{C_D}$ presents a 18.65% overestimation compared with the experimental result. The difference is mainly because of no dissipation of Reynolds stress in the spanwise direction [8]. It results in vortex forming closer to the body back so that the pressure on the back surface is lower. The overestimation in drag is inherent for two-dimensional direct simulation performing in cylinder flow at a high Reynolds number.

Tab. 2 shows C_D values of typical cylindrical bodies, i.e. circular and square cylinders, and present body, from both experiments and two-dimensional direct numerical simulations (DNS). For circular cylinder at $Re = 10\,000$, the overestimation is 14.8%~15.9% [9-10]. And for square cylinder at $Re = 21\,400$, the overestimation is 17.6% [11-12]. The overestimation of the present calculation is 18.7%, which is comparable to those of the typical cylindrical bodies. For the Strouhal number, the value shows an agreement with the experiment result with a 9.57%. Therefore, the difference of the present calculation and the experiment is considered to be normal. The capability for capturing dominant flow structures in a kinetic point of view is verified.

2 Results and discussion

All the data used in the analysis are captured after $t = 200$, when the calculation has reached time stationary.

2.1 Drag and lift

Fig. 2 shows time histories of the drag coefficient C_D and the lift coefficient C_L. C_L shows a periodic shows the spectra of two signals. The spectra are calculated by Fast Fourier Transform (FFT) using 5×10^4 sampling data from $t = 250$ to 500. The spectrum of C_L presents dominant peaks at two closing values of $f_L = 0.236$ and 0.256, approximately equal to St. As splitting the C_L signal into multiple windows of $\Delta t = 30$, the peak value appears to switch between 0.236 and 0.256. The same phenomenon was observed in the work of Parkin [2]. For majority of sampling windows, the dominant peak is at $f_L = 0.256$. The spectrum of the

The C_D signal presents various frequency components. A peak at $f_D = 0.492$ is observed,

Tab. 1. Results of the present calculation and the previous experimental and numerical studies.

Study	Method	Re	δ	H_{12}	$\overline{C_D}$	St
A	Exp.	23 000	0.22	1.19	0.98	0.23
B	LES	20 000	/	/	1.02	0.31
C	LES	23 000	/	/	0.72	0.22
P	DNS	23 000	0.25	1.46	1.163	0.252

Tab. 2 $\overline{C_D}$ **values of circular cylinder, square cylinder, and the present body obtained from experiments and two-dimensional (2-D) DNS.**

geometry	*Re*	Exp.	2-D DNS
gircular cylinder	10 000	0.966 [9]	1.109～1.120 [10]
square cylinder	21 400	2.05 [11]	2.41 [12]
the present body	23 000	0.98 [3]	1.163

which is approximately equal to two times of the dominant lift frequency. It suggests the trailing-edge tvortex is dominated by the wake instability, where each lift period represents two shed vortices, while each drag period represents one.

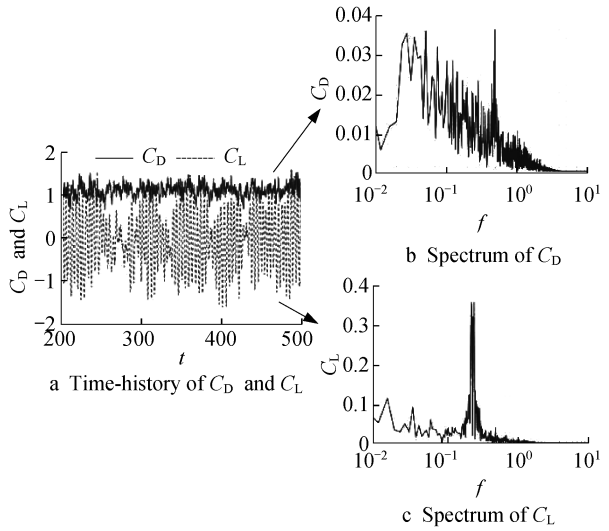

Fig. 2 Time history of C_D **and** C_L**, together with spectra of the signals**

Some minor peaks occur at low-value region $f<0.1$, which indicates a low-frequency oscillation of C_L. Correspondingly, the amplitude of the fuctuation varies with a long-time-scale period. The same variation is observed in the three-dimensional simulation of Parkin [2]. It indicates the low-frequency oscillation of the lift fluctuation is a two-dimensional flow feature. The fluctuation shows low-amplitude periods around 270, 330, 390, and 430.

Tab. 3 presents properties of the drag and the lift calculated during both of a high- and a low-amplitude periods. C_D for the high-amplitude period is 2.95% higher than that for the ow-amplitude period. The fluctuation of drag and lift for the high-amplitude periods are, respectively, 14.03% and 24.68% higher than those for the low-amplitude period. Dominant frequency for lift does not change in two periods. While the drag for the low-amplitude period shows a broad-band feature with no dominant frequency.

Tab. 3 Drag and lift coefficients during the periods of the alternative- and the simultaneous vortex shedding

period	high-amplitude	low-amplitude
sampling time t	473.8～523.5	402.2～453.9
$\overline{C_D}$	1.168 0	1.134 5
$C_{D\,rms}'$	0.154 4	0.135 4
f_D	0.51	/
$C_{L\,rms}'$	0.827 5	0.663 7
f_L	0.24	0.24

2.2 Wake dynamics

Fig. 4 shows the wake evolution around $t=430$, represented by instantaneous vorticity field captured at $t=425$～435 with a time interval of $\Delta t=2$. The corresponding time history of C_D and C_L are presented as a reference. For $t=425$ to 427, the separated shear layers at back shed vortices from the upper sides. Correspondingly, C_L rises from lower value to higher value. The wake presents a typical von Karman wake. For $t=427$ to 430, the phase difference between the upper and the lower vortices is attenuated gradually to null. The separated shear layers roll up at symmetric places to the center line and shed vortices simultaneously. Correspondingly, C_L oscillates within a lower amplitude. It is mainly because of the canceling effect of simultaneous vortex shedding. For $t=430$ to 433, the upper and lower shear layer interacts at the center line. Subsequently, a single vortex is shed from the upper side at $t=435$, indicating the alternative shedding feature recovers. Correspondingly, C_L experiences a positive peak and the amplitude of fluctuation increases. The evolution of flow structures from $t=425$ to 435 indicates that the vortex shedding in the wake switches between two modes: the alternative and the simultaneous shedding modes. When the vortex is shed simultaneously/alternatively, the amplitude of C_L

fluctuation is lower/ higher.

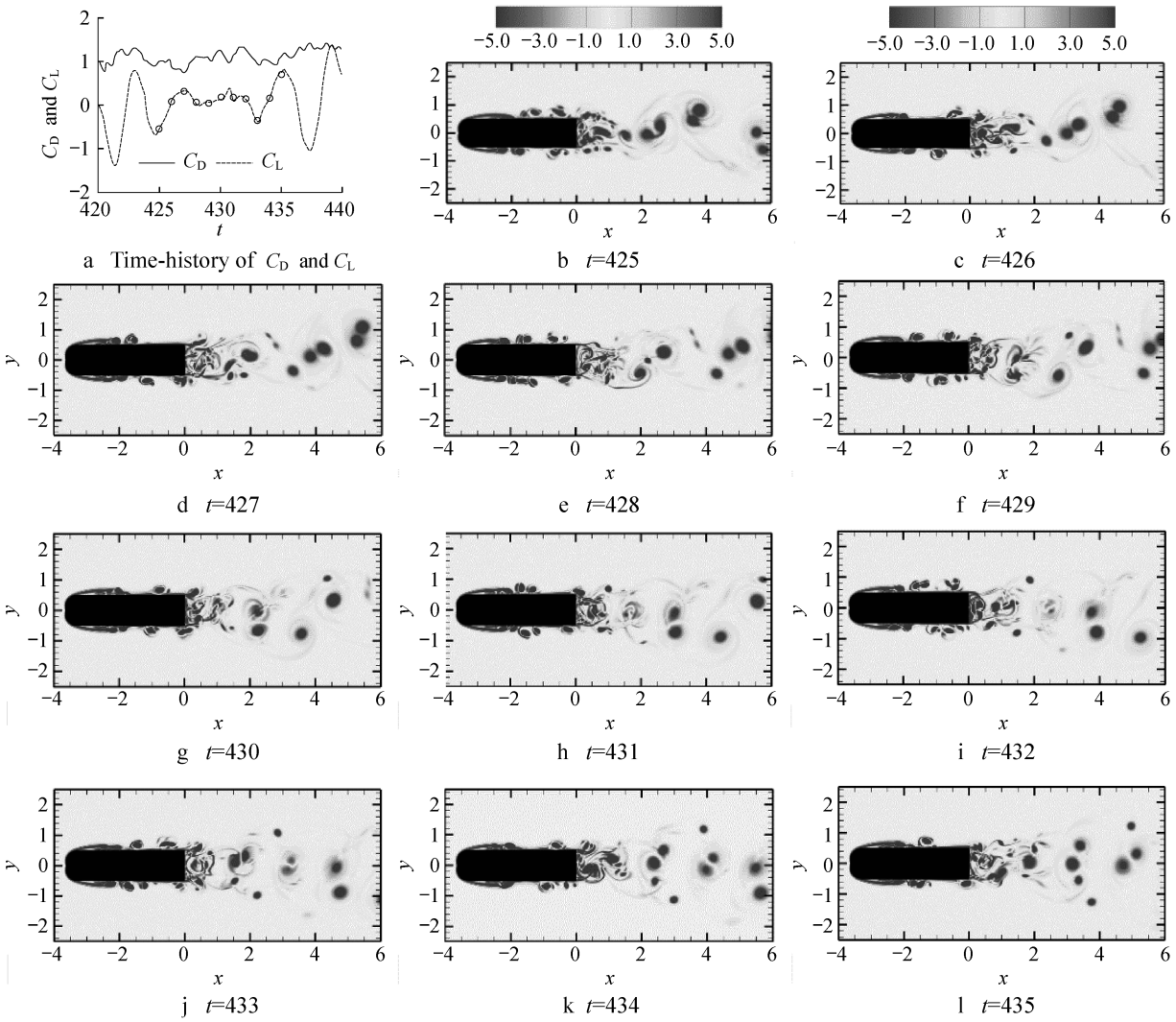

Fig. 4 Instantaneous vorticity distribution cpatured from $t=425$ to 435, together with time-history of C_D and C_L.

2.3 On the control mechanism

Fig. 5 shows time-history of the streamwise velocity u measured at the upper and the lower shear

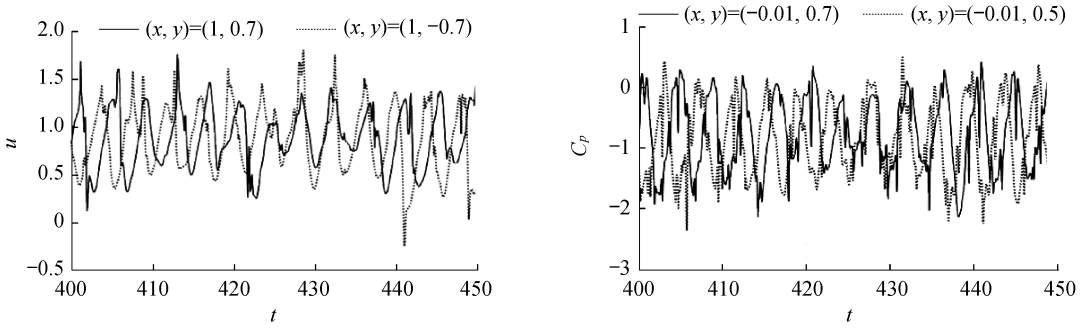

Fig. 5 Time history of streamwise velocity and surface pressure coefficient measured, respectively, at $(x,y)=(1,\pm0.7)$ and $(x,y)=(-0.01,\pm0.5)$.

layers at $(x, y) = (1, \pm 0.7)$, and the surface pressure coefficient C_p measured at two trailing edges at $(x, y) = (-0.01, \pm 0.7)$. The velocity fluctuation of the upper and the lower shear layer presents the same phase around $t = 430$, indicating the upper and the lower vortices are shed from respective trailing edges at the same phase. Correspondingly, the surface pressure coefficient fluctuation acting on the upper and the lower trailing edges shows the same phase around $t = 430$, indicating the pressure pulses acting on two sides have the same phase. As a result, the pressure difference between the upper and the lower sides is cancelled out. And the lift fluctuation is attenuated.

According to the instability analysis [12], the shear layer is governed by the Kelvin-Helmholtz instability. At the initial stage of separation, the upper and the lower shear layers have no interaction. And vortices are shed simultaneously. As the vortices travel to the far wake, where the Benard-Karman instability dominates, they interact and travel in an alternating order. The asymmetric feature propagates upstream, subsequently, resulting in the interacting shear layers. In the present flow, both the alternative and the symmetric vortex shedding are observed, suggesting the Benard-Karman instability does not totally overwhelm the Kelvin-Helmholtz instability. It is probably because the separated shear layer achieves more energy from the turbulent boundary layer to resist the wake instability.

3 Conclusions and outlooks

A low-frequency oscillation in the wake of a two-dimensional generic vehicle profile has been numerically studied. The simulation has shown good capability for capturing dominant flow structures in a kinetic point of view. Results have shown larger lift fluctuation occurs as vortices are shed alternatively from the trailing edge, while weaker fluctuation occurs as the vortices are shed simultaneously. The attenuated fluctuation results from the cancelling effect of the upper and the lower surface pressure. The imbalance of the Benard-Karman instability in the wake and the Kelvin-Helmholtz instability in the shear layer may cause the switch of the shedding modes. And the switch leads to the low-frequency oscillation in the lift signal.

Reference:

[1] HUCHO W, SOVRAN G. Aerodynamics of road vehicles [J]. Annual Review of Fluid Mechanics, 1993, 25(1): 485.

[2] PARKIN D J, THOMPSON M C, SHERIDAN J. Numerical analysis of bluff body wakes under periodic open-loop control [J]. Journal of Fluid Mechanics, 2014, 739: 94.

[3] PASTOOR M, HENNING L, NOACK B R, *et al*. Feedback shear layer control for bluff body drag reduction [J]. Journal of Fluid Mechanics, 2008, 608: 161.

[4] LAM G C, LEUNG R C, SEID K H, *et al*. Validation of CE/SE scheme in low mach number direct aeroacoustic simulation [J]. International Journal of Nonlinear Sciences and Numerical Simulation, 2014, 15(2): 157.

[5] LAM G C Y, LEUNG R C K, TANG S K. Aeroacoustics of T-junction merging flow [J]. The Journal of the Acoustical Society of America, 2013, 133(2): 697.

[6] SEID K H, GILKA G, LEUNG R. *et al*. A comparison study of reduced order models for aeroacoustic applications [C]// 18th AIAA/CEAS Aeroacoustics Conference. [S. l.]: American Institute of Aeronautics and Astronautics, 2012: 2072-2103.

[7] KRAJNOVIĆ S, FERNANDES J. Numerical simulation of the flow around a simplified vehicle model with active flow control[J]. International Journal of Heat and Fluid Flow, 2011, 32(1): 192.

[8] MITTAL R, BALACHANDAR S. Effect of three-dimensionality on the lift and drag of nominally two-dimensional cylinders [J]. Physics of Fluids, 1995, 7(8): 1841.

[9] ROSHKO A. Experiments on the flow past a circular cylinder at very high Reynolds number [J]. Journal of Fluid Mechanics, 1961, 10(3): 345.

[10] BRAZA M, CHASSAING P, MINH H H. Prediction of large-scale transition features in the wake of a circular cylinder [J]. Physics of Fluids A: Fluid Dynamics, 1990, 2(8): 1461.

[11] LYN D A, EINAV S, RODI W, *et al*. A laser-Doppler velocimetry study of ensemble-averaged characteristics of the turbulent near wake of a square cylinder [J]. Journal of Fluid Mechanics, 1995, 304: 285.

[12] HUERRE P, MONKEWITZ P A. Local and global instabilities inspatially developing flows [J]. Annual Review of Fluid Mechanics, 1990, 22(1): 473.